

---

## On necessary pumping pressures for industrial process-driven particle-laden fluid flows

T. I. Zohdi

Department of Mechanical Engineering  
University of California  
Berkeley, CA, 94720-1740, USA

### Abstract

Due to increasing demands for faster and faster manufacturing of new complex materials, such as casting of particulate composites, the determination of pumping pressures needed for particle-laden fluids through channels is critical. In particular, the increase in viscosity as a function of the particle volume fraction can lead to system malfunction, due to an inability to deliver necessary pressures to pump the more viscous fluid through the system. This paper studies the pressure gradient needed to maintain a given flow rate, explicitly as a function of the volume fraction of particles present in the fluid. It is also crucial to control voids in the casted products, which can be traced to air-entrainment, spurious internal reactions, de-wetting, etc, which can be traced to high Reynolds numbers. Accordingly, an expression for the resulting Reynolds number as a function of the particle volume fraction and flow rate is also developed. Numerical examples are provided to illustrate the practical use of the derived relations to characterize the necessary pumping pressures for process-driven, particle-laden fluid flows.

## 1 Introduction

In a variety of industries, ranging from next generation engines, turbo machinery, printed electronics, food processing, etc, new types of heterogeneous materials, comprised of particulates in a binding matrix, are being developed and utilized. The macroscopic material characteristics of the material are dictated by the aggregate response of an assemblage of particles suspended in a binding matrix material. In the fabrication of such materials, the basic philosophy is to select material combinations to produce desired aggregate responses. For example, in structural engineering applications, the classical choice is a harder particulate phase that serves as a stiffening agent for a ductile, easy to form, base matrix material. Oftentimes, such materials start in particulate form, and are then mixed with a binder and delivered as a flowing slurry to be cast into their final shape.<sup>1</sup> Thus, because of the increasing demands for faster and faster manufacturing of new complex particle-laden materials, the determination of pumping pressures needed to move such fluids through channels is critical (Figure 1).

For particle laden fluids delivered through channels, the increase in viscosity can lead to system malfunction, due to an inability to supply necessary pressures

<sup>1</sup>Over 50 % (by mass) of man-made materials start in granulated form.

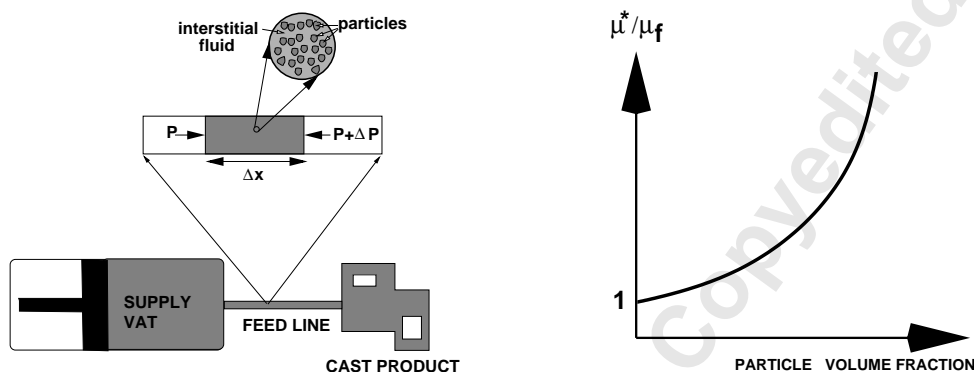


Figure 1: (a) A particle laden fluid in a channel and (b) the increase in the ratio of effective viscosity to baseline fluid viscosity ( $\mu^*/\mu_f$ ) as a function of secondary particle volume fraction ( $\nu_p$ ).

to pump the more viscous material properly. This paper studies the pressure gradient needed to maintain a given flow rate, explicitly as a function of the volume fraction of particles present in the fluid. The expression is general and easy to apply for the analysis of pumping particle-laden fluids. Furthermore, it is crucial to control voids in the resulting casted products, which are correlated to air-entrainment, spurious internal reactions, de-wetting, etc. These effects are correlated to high Reynolds numbers. Accordingly, an expression for the resulting Reynolds number as a function of the particle volume fraction and flow rate is also developed. Numerical examples are provided to illustrate the practical use of the derived relations to characterize the necessary pumping pressures for process-driven particle-laden fluid flows. Because resulting voids may be impossible to avoid, we also determine their effects on the overall effective properties of a heterogeneous two-phase slurry consisting of particles and a binding interstitial material. Estimates are developed for the reduction of the overall mechanical and thermal properties, based on embedded, double application of the Hashin-Shtrikman bounds, whereby, on the first level, the effective properties due to voids are computed, and on the second level the smaller scale heterogeneous material is taken into account.<sup>2</sup>This research is also quite relevant to the development of high-resolution electrohydrodynamic-jet printing processes. For overviews, see Wei and Dong [1], who also develop specialized processes employing phase-change inks. Such processes are capable of producing micron-level footprints for high-resolution additive manufacturing.

<sup>2</sup>Generally, use of homogenized effective properties is justified if the inherent length scale ratio of the particles to the structure is below 1:50.

**Remark:** The objective of the analysis is to develop semianalytical expressions that can help guide analysts who are designing manufacturing systems involving particle-laden flows. Clearly, one could approach the problem with a large-scale CFD analysis. However, for direct numerical simulation of particle-laden continua, spatio-temporal discretization grids must be extremely fine, with several thousand numerical unknowns needed per particle length-scale for numerically-accurate results. Thus, for several hundred thousand particles in a system a proper discretization would require several billion numerical unknowns (see for example Onate et al. [2, 3], Rojek et al. [4], Carbonell et al. [5], Labra and Onate [6], Leonardi et al [7], Cante et al [8], Rojek [9], Onate et al [10], Bolintineanu et al [11], Avci and Wriggers [12] and Zohdi [13, 14] and Zohdi and Wriggers [15]). Although such simulations are possible in high-performance computing centers, their usefulness for rapid daily design analysis is minimal. This will be discussed further in the summary.

## 2 Channel flow

As indicated in the introduction, the presence of secondary particles in fluids, particularly within channels, is wide-ranging and their presence can dramatically increase the effective overall viscosity, thus requiring increased applied pressure to maintain nominal flow rates (Figure 1). The primary objective of the first part of this analysis is to derive a relatively easy to use expression for the pressure gradient required to maintain a given flow rate in a channel, as a function of the volume fraction of secondary particles present in the fluid.

Accordingly, consider an idealized channel with a circular cross-section of area  $A = \pi R^2$ , with a velocity profile given by a classical channel-flow of the form:

$$v = v_{\max} \left( 1 - \left( \frac{r}{R} \right)^q \right), \quad (1)$$

where  $v_{\max}$  is the centerline velocity and  $r$  is the radial coordinate from the centerline of the channel. For fully developed laminar flow,  $q = 2$ , while for increasing  $q$  one characterizes, phenomenologically, progressively turbulent flow ( $q \geq 2$ ). The shear stress is given by

$$\tau = \mu^* \frac{\partial v}{\partial r} = -\frac{\mu^* v_{\max} q}{R} \left( \frac{r}{R} \right)^{q-1}, \quad (2)$$

where  $\mu^*$  is the effective viscosity of the particle-laden fluid. We assume that the overall flow rate is assumed constant, thus

$$Q = \int_A v dA = Q_o. \quad (3)$$

One can show that

$$v_{\max} = \frac{Q_o(q+2)}{Aq} = \frac{Q_o(q+2)}{\pi R^2 q}. \quad (4)$$

The stress at the wall becomes

$$\tau_w = -\tau(r = R) = \frac{\mu^* v_{\max} q}{R} = \frac{\mu^* Q_o (q + 2)}{\pi R^3}. \quad (5)$$

We have the following observations:

- Increasing  $\mu^*$ ,  $Q_o$  or  $q$  increases the stress at the wall ( $\tau_w$ ),
- Increasing  $q$  leads to an increasingly more blunted flow profile and
- Decreasing  $R$  increases the stress at the wall ( $\tau_w$ ).

**Remarks:** In the remaining analysis, we will assume steady flow, the particles are not elongated and that they are well distributed within the base fluid.<sup>3</sup> Furthermore, we will adopt a generalization of the classical Poiseuille solution for fully developed flow in a pipe (assuming the velocity depends on some undetermined power  $q$  instead of the standard parabolic dependence for laminar single-phase flow).

### 3 Pressure gradients

The previous expressions allow us to correlate the pressure applied to a volume of particle-laden to allow it to move as a constant flow rate. By performing a force balance we have in the positive  $x$ -direction (assuming steady flow, no acceleration)

$$(-(P + \Delta P) + P)\pi R^2 - \tau_w 2\pi R \Delta x = 0, \quad (6)$$

where  $x$  is the coordinate along the length of the channel and  $\Delta x$  is the differential length, leading to

$$-\Delta P = \mu^* \frac{Q_o (q + 2)}{\pi^2 R^5} 2\pi R \Delta x = \frac{2\mu^* Q_o (q + 2) \Delta x}{\pi R^4}, \quad (7)$$

where we used the expression for  $v_{\max}$  and where the effective viscosity is a function of the volume fraction of particles,  $\mu^* = \mu^*(\nu_p)$ . An explicit relation for  $\mu^*(\nu_p)$  will be given shortly. Solving for the pressure gradient yields

$$-\frac{\Delta P}{\Delta x} = \underbrace{\frac{2\mu^*(q + 2)}{\pi R^4}}_C Q_o \stackrel{\text{def}}{=} C Q_o. \quad (8)$$

If we fix the flow rate  $Q_o$ , the multiplier  $C$  identifies the pressure gradient needed to achieve a flow rate  $Q_o$ . For a fixed value of  $q$ , the expression directly indicates that an increase in viscosity will require an increase in the pressure gradient.

<sup>3</sup>In long channels, elongated particles can tend to align themselves in a particular direction that could also affect their viscosity. The assumptions made eliminate this possibility for the problems under consideration.

For small channels this can be a problem, as indicated by the  $R^4$  term in the denominator. However, in general,  $q$  is a function of the Reynolds number. This case will be considered next.

## 4 Velocity profile characteristics

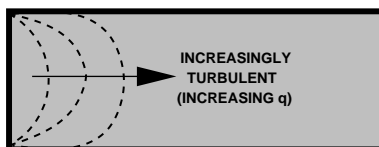


Figure 2: Progressive blunting of the velocity profile with increasing Reynolds number.

As the Reynolds number increases, the velocity profile will change from a quadratic ( $q = 2$ ) to a more blunted profile ( $q \gg 2$ ), which represents, phenomenologically, turbulent (inertia-dominated) behavior (Figure 2). The effect of a changing profile is described by representing  $q$  by a linear function of the centerline Reynolds' number ( $\mathcal{R}_{ec}$ )

$$q = q(\mathcal{R}_{ec}) = c_1 \mathcal{R}_{ec} + c_2, \quad (9)$$

where  $\mathcal{R}_{ec} = \frac{\rho^* v_{max} 2R}{\mu^*}$  and  $c_1$  and  $c_2$  are constants. Models of this type, linking the profile exponent ( $q$ ) to the centerline Reynolds' number ( $\mathcal{R}_{ec}$ ), are quite well-established, for example, see Hinze [16]. Usually,  $0 \leq c_1 \ll 1$  and  $c_2 \approx 2$ , and in the limit we have, for  $c_1 = 0$  and  $c_2 = 2$ , laminar flow ( $q = 2$ ). For the general case, combining Equation 4 with Equation 9 and the definition of the centerline Reynolds' number, we obtain a quadratic relationship for  $q$ ,

$$q^2 - (\gamma^* + c_2)q - 2\gamma^* = 0, \quad (10)$$

where  $\gamma^* = \frac{2c_1 Q_o \rho^*}{\pi R \mu^*}$ , where  $\rho^*$  is the effective density and  $\mu^*$  is the effective viscosity. This quadratic relationship can be solved in closed form for  $q$  to yield<sup>4</sup>

$$q(\mathcal{R}_{ec}) = \frac{1}{2} \left( (\gamma^* + c_2) \pm \sqrt{(\gamma^* + c_2)^2 + 8\gamma^*} \right). \quad (11)$$

<sup>4</sup>In the special case of laminar flow ( $c_1 = 0$  and  $c_2 = 2$ ) there are two roots to Equation 16,  $q = 2$  and  $q = 0$ .

---

The larger root is the physically correct choice (since the smaller root can become negative). We further observe that  $q(\mathcal{R}_{ec})$  is a function of  $R^{-1}$  and decreasing  $R$  increases  $q$ , for fixed  $Q_o$ .

## 5 Models for effective properties of particle-laden fluids

It is important to be able to characterize the effective properties of a particle-laden fluid as a function of the volume fraction of particles and the baseline (interstitial) fluid properties. The density of the particle-laden fluid is actually an “effective density”, since it actually is a mixture of materials (particles and interstitial fluid). Effective properties are defined through volume averages. For example, the effective density of the mixture is

$$\rho^* \stackrel{\text{def}}{=} \langle \rho(\mathbf{x}) \rangle_V \stackrel{\text{def}}{=} \frac{1}{V} \int_V \rho(\mathbf{x}) dV = \frac{1}{V} \left( \int_{V_f} \rho_f dV + \int_{V_p} \rho_p dV \right) = \nu_f \rho_f + \nu_p \rho_p \quad (12)$$

where  $\nu_f$  and  $\nu_p$  are the volume fractions of the fluid and particles, respectively. The volume fractions have to sum to unity:

$$\nu_f + \nu_p = 1 \Rightarrow \nu_f = 1 - \nu_p \quad (13)$$

Similar approaches can be used to calculate various types of properties, such as the effective viscosity (a transport property). However, to calculate them is a bit more complicated, since they require one to estimate the types of interaction between the constituents. There are a number of models which provide expressions for the effective viscosity of the fluid containing particles. For the purposes of this flow analysis, the particles are considered to be rigid, relative to the surrounding fluid. For example, in 1906, Einstein [17] developed an approximation which is quite simple, but only valid at extremely low volume fractions of particles (under one percent). It reads as

$$\mu^* = \mu_f(1 + 2.5\nu_p), \quad (14)$$

where  $\mu_f$  is the viscosity of the surrounding (incompressible) fluid and the particles are assumed rigid. At even quite moderate to high volume fractions, this approximation is inaccurate. A better approximation, which is in fact a rigorous lower bound on the effective viscosity, can be derived from the well-known Hashin and Shtrikman [18-20] bounds (see appendix), and reads as:

$$\mu^* = \mu_f \left( 1 + 2.5 \frac{\nu_p}{1 - \nu_p} \right). \quad (15)$$

The expression above is the tightest known lower bound on the effective viscosity of a two-phase material comprised of rigid particles in a surrounding incompressible fluid. The origin of the expression in Equation 15 stems from

bounds on effective responses for solid two-phase mixtures (see appendix). This expression remains quite accurate up to about  $\nu_p = 0.25$ , which is sufficient for most applications and allows us to directly correlate the pressure gradient to the volume fraction of the particles. We refer the reader to Torquato [21] for more details.

## 6 Correlation of pressure gradient to particle volume fraction

Using the effective properties, we have an expression for the velocity profile exponent

$$q(\mathcal{R}_{ec}(\mu^*, \rho^*), \gamma^*) = \frac{1}{2} \left( (\gamma^* + c_2) \pm \sqrt{(\gamma^* + c_2)^2 + 8\gamma^*} \right). \quad (16)$$

Consequently, the pressure gradient's dependency on the volume fraction of particles can be written as

$$-\frac{\Delta P}{\Delta x} = \frac{2(\mu_f(1 + 2.5\frac{\nu_p}{1-\nu_p})) (q(\mathcal{R}_{ec}(\mu^*, \rho^*), \gamma^*) + 2)}{\pi R^4} Q_o \stackrel{\text{def}}{=} C^* Q_o, \quad (17)$$

where  $C^* = C^*(Q_o)$ . For a fixed flow rate,  $Q_o$ , increasing the volume fraction of particles ( $\nu_p$ ) requires a corresponding increase in the pressure differential. Explicitly, the Reynolds number is

$$Re = \frac{v_{max} D \rho^*}{\mu^*} = \frac{2Q_o(q+2)}{\pi R q} \frac{((1-\nu_p)\rho_f + \nu_p\rho_p)}{\mu_f(1 + 2.5\frac{\nu_p}{1-\nu_p})}. \quad (18)$$

## 7 Trends

To illustrate the trends, we varied  $Q_o$  from  $10^{-3} m^3/s$  to  $10^{-2} m^3/s$  and utilized the expression in Equation 17. We plotted the pressure gradient and Reynolds number as a function of the volumetric flow rate ( $Q_o$ ) in Figure 3 for various values of  $\nu_p$ , with the following parameters used:<sup>5</sup>

- Viscosity:  $\mu_f = 0.01 Pa - s$ ,
- Fluid density:  $\rho_f = 2000 kg/m^3$ ,
- Particle density:  $\rho_p = 5000 kg/m^3$ ,
- Channel radius:  $R = 0.01 m$ , and
- Profile constants:  $c_1 = 0.01$  and  $c_2 = 2$ .

<sup>5</sup>For reference, the viscosity of water is  $\mu_f = 0.001 Pa - s$  and for honey is  $\mu_f = 1 Pa - s$ .

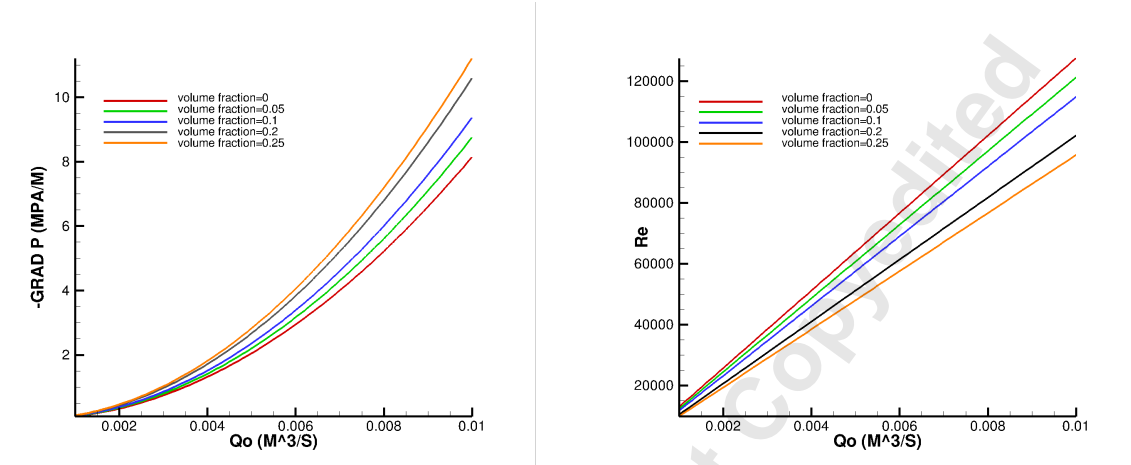


Figure 3: TRENDS: LEFT: The pressure gradient needed ( $-\frac{\Delta P}{\Delta x}$ ) as a function of the desired volumetric flow rate ( $Q_o$ ) for various volume fractions of  $\nu_p$ . RIGHT: The resulting Reynolds number as a function of the volumetric flow rate ( $Q_o$ ).

Generally, the trends are that a steady increase in the pressure gradient (approximately 40 % more) is needed to maintain a fixed  $Q_o$ , for increasing volume fraction of particles. Due to the increase in the particle volume fraction, the viscosity increases, thus decreasing the Reynolds number. High Reynolds numbers, and consequential turbulence, can lead to aspiration (air entrainment), spurious internal reactions, de-wetting, etc, which can lead to voids. The point of this example was not to illustrate an all encompassing parameter set, but simply to show the explicit dependency of the pressure gradient and Reynolds number on the presence of secondary particles. Other parameter sets can be easily simulated.

## 8 Summary

The presence of particle-laden fluids is widespread. Because the presence of particles increases the overall viscosity of the fluid, the pressure gradients needed to pump such fluids through channels at a nominal flow rate can increase dramatically. The present analysis and model can provide a useful guide to designing systems that pump particle laden flows, with the purpose to be able to cast materials. This paper derived the pressure gradient needed to maintain a given flow rate, as a function volume fraction of particles present in the fluid. The expression explicitly correlates the dependency of the pressure gradient to the particle volume fraction, and is hopefully easy to use by researchers in the field.

Furthermore, the developed expressions also provide estimates on the Reynolds numbers that arise for given flow rates. The tracking of the Reynolds number is important, since turbulence can lead to improper casting due to the resulting voids. For example, one can estimate the reduction of the material quality as a function of the porous material by assuming that it is comprised of an isotropic elastic matrix, with a bulk modulus  $\kappa_m$  and shear modulus  $\mu_m$ , while the porous void space is modeled by an elastic material with very low bulk and shear moduli  $\kappa_v = \delta\kappa_m$ ,  $\mu_v = \delta\mu_m$ , with  $0 \leq \delta \ll 1$ . The exact case of voids corresponds to  $\delta \rightarrow 0$ . To estimate the properties of the material with voids, we employ the Hashin-Shtrikman bounds (see appendix), assign the following (the harder material is the matrix and the softer is the voids):  $\kappa_v = \kappa_1$ ,  $\mu_v = \mu_1$  and  $\kappa_m = \kappa_2$ ,  $\mu_m = \mu_2$ ,  $\nu_v = \nu_1$  and  $\nu_m = \nu_2$ , and force  $\mu_v \rightarrow 0$  and  $\kappa_v \rightarrow 0$  to obtain

$$0 \leq \kappa^{*,voids} \leq \kappa_m(1 - \nu_v G(\nu_v)) \quad (19)$$

where

$$G(\nu_v) = \frac{3\kappa_m + 4\mu_m}{3\nu_v\kappa_m + 4\mu_m} \quad (20)$$

and

$$0 \leq \mu^{*,voids} \leq \mu_m(1 - \nu_v C(\nu_v)) \quad (21)$$

where

$$C(\nu_v) = \frac{5(3\kappa_m + 4\mu_m)}{\kappa_m(9 + 6\nu_v) + \mu_m(8 + 12\nu_v)}. \quad (22)$$

One can then assign the effective properties of the void-free part of the particle-laden mixture to the matrix material,  $\kappa^{*,no-voids} = \kappa_m$  and  $\mu^{*,no-voids} = \mu_m$ , leading to

$$0 \leq \kappa^{*,voids} \leq \kappa^{*,no-voids}(1 - \nu_v G(\nu_v)) \quad (23)$$

and

$$0 \leq \mu^{*,voids} \leq \mu^{*,no-voids}(1 - \nu_v C(\nu_v)). \quad (24)$$

It is important to note that

- As  $\nu_v \rightarrow 1$ ,  $\nu_v G(\nu_v) \rightarrow 1$  and  $\nu_v C(\nu_v) \rightarrow 1$ , thus  $\mu^{*,voids} \rightarrow 0$  and
- As  $\nu_v \rightarrow 0$ ,  $\nu_v G(\nu_v) \rightarrow 0$  and  $\nu_v C(\nu_v) \rightarrow 0$ , thus  $\mu^{*,voids} \rightarrow \mu^{*,no-voids}$ .

These expressions show the resulting effective property loss as a function of the voids. Further expressions on the reduction of material performance are provided in Appendix 2. We remark that in some applications, such as biomedical devices, controlled porosity with pre-specified pore shapes, sizes and distributions are sought after using, for example, Porogen Templating Processes. We

---

refer the reader to Hong et al [22] for a detailed overview of the state of the art of porogen patterning. Other emerging, cutting-edge, approaches for controlled generation of desired porosity involve laser processing (Kongsuwan et al [23]). This is particularly useful for precisely functionalized layered substrates.

In summary, the present analysis and model can provide a useful guide to designing and interpreting experiments. However, while the model can provide qualitative information, extensions are almost certainly going to require complex spatio-temporal discretization resolving multiparticle particle-fluid interaction. Such particle/fluid systems are strongly coupled, due to the drag forces induced by the fluid onto the particles and vice-versa. For example, in Zohdi [13, 14], a flexible and robust solution strategy was developed to resolve coupled systems comprised of large groups of flowing particles embedded within a continuous flowing fluid. The focus of that work was to develop adaptive time stepping schemes which properly resolve the coupling, via a staggered recursive time-stepping process. The approach can be used in conjunction with computational fluid mechanics codes based on finite difference, finite element, finite volume or discrete element discretization, for example such as those developed in Onate et al. [2, 3], Rojek et al. [4], Carbonell et al. [5], Labra and Onate [6], Leonardi et al [7], Cante et al [8], Rojek [9], Onate et al [10], Bolintineanu et al [11], Avci and Wriggers [12] and Zohdi [24-26]. Finally, we mention that oftentimes the detrimental growth of channel walls (thus clogging feed lines) starts with the adhesion of particles to the surfaces. This is a complex process, which is likely to involve low fluid-induced shear stress (allowing particles stick to the walls, Zohdi [27, 28], Zohdi et al [29]) and strongly coupled diffusive, chemical effects and thermal effects. The application of such computational procedures to the problems considered in this paper is under current investigation by the author.

## 9 References

1. Wei, C. and Dong, J. 2014. Development and Modeling of Melt Electrohydrodynamic-Jet Printing of Phase-Change Inks for High-Resolution Additive Manufacturing, *J. Manuf. Sci. Eng.* 136, 061010; Paper No: MANU-14-1179; doi:10.1115/1.4028483.
2. Onate, E., Idelsohn, S. R., Celigueta, M. A. and Rossi, R. 2008. Advances in the particle finite element method for the analysis of fluid-multibody interaction and bed erosion in free surface flows. *Computer Methods in Applied Mechanics and Engineering*, Vol. 197 (19-20), pp. 1777-1800.
3. Onate, E. and Celigueta, M. A. and Idelsohn, S. R. and Salazar, F. and Suarez, B. 2011. Possibilities of the Particle Finite Element Method for fluid-soil-structure interaction problems, *Computational Mechanics*, Vol. 48, 307-318.
4. Rojek J., Labra C., Su, O. and Onate, E. 2012. Comparative study of different discrete element models and evaluation of equivalent micromechanical parameters, *International Journal of Solids and Structures*, Vol 49, pp. 1497-1517, 2012 DOI: 10.1016/j.ijsolstr.2012.02.032.
5. Carbonell, J.M., Onate E. and Suarez B. 2010. Modeling of ground excavation with the particle finite element method. *Journal of Engineering Mechanics*, ASCE, Vol. 136, pp. 455-463.

6. Labra, C. and Onate E. 2009. High-density sphere packing for discrete element method simulations. *Communications in Numerical Methods in Engineering*, Vol. 25 (7), pp. 837-849.
7. Leonardi, A., Wittel, F. K., Mendoza, M and Herrmann, H. J. 2014. Coupled DEM-LBM method for the free-surface simulation of heterogeneous suspensions. *Computational Particle Mechanics*, Volume 1, Issue 1, pp 3-13.
8. Cante, J., Davalos, C., Hernandez, J. A., Oliver, J., Jonsen, P., Gustafsson, G., Haggblad, H. A. 2014. PFEM-based modeling of industrial granular flows. *Computational Particle Mechanics*, Volume 1, Issue 1, pp 47-70.
9. Rojek, J. 2014. Discrete element thermomechanical modelling of rock cutting with valuation of tool wear. *Computational Particle Mechanics*, Volume 1, Issue 1, pp 71-84.
10. Onate, E., Celigueta, M. A., Latorre, S., Casas, G., Rossi, R. and Rojek, J. 2014. Lagrangian analysis of multiscale particulate flows with the particle finite element method *Computational Particle Mechanics*, Volume 1, Issue 1, pp 85-102.
11. Bolintineanu, D. S., Grest, G. S., Lechman, J. B., Pierce, F., Plimpton, S. J. and Schunk, P. R. 2014. Particle dynamics modeling methods for colloid suspensions. *Computational Particle Mechanics*, Volume 1, Issue 3, pp 321-356.
12. Avci, B. and Wriggers, P. 2012. A DEM-FEM coupling approach for the direct numerical simulation of 3D particulate flows, *Journal of Applied Mechanics*, Vol. 79, 010901-1-7.
13. Zohdi, T. I. 2007. Computation of strongly coupled multifield interaction in particle-fluid systems. *Computer Methods in Applied Mechanics and Engineering*. Volume 196, 3927-3950.
14. Zohdi, T. I. 2014. Embedded electromagnetically sensitive particle motion in functionalized fluids. *Computational Particle Mechanics*. Vol 1, 27-45.
15. Zohdi, T. I. and Wriggers, P. 2008. Introduction to computational micromechanics. Springer-Verlag.
16. Hinze, J. O. 1975. Turbulence. McGraw-Hill. New York
17. Einstein, A. 1906. A new determination of molecular dimensions. *Annals of Physics*, 19(4), 289306.
18. Hashin, Z. and Shtrikman, S. 1962. On some variational principles in anisotropic and nonhomogeneous elasticity. *Journal of the Mechanics and Physics of Solids*. **10**, 335-342.
19. Hashin, Z. and Shtrikman, S. 1963. A variational approach to the theory of the elastic behaviour of multiphase materials. *Journal of the Mechanics and Physics of Solids*. **11**, 127-140.
20. Hashin, Z. 1983. Analysis of composite materials: a survey. *ASME Journal of Applied Mechanics*. **50**, 481-505.
21. Torquato, S. 2002. *Random Heterogeneous Materials: Microstructure & Macroscopic Properties* Springer-Verlag, New York.
22. Hong, Y., Zhou, J. G. and Yao, D. 2014. Porogen Templating Processes: An Overview. *J. Manuf. Sci. Eng.* 136(3), Paper No: MANU-13-1304; doi: 10.1115/1.4026899.
23. Kongsuwan, P., Brandal, G. and Yao, Y. L. 2015. Laser Induced Porosity and Crystallinity Modification of a Bioactive Glass Coating on Titanium Substrates. *J. Manuf. Sci. Eng.* 137(3), Paper No: MANU-14-1245; doi: 10.1115/1.4029566.
24. Zohdi, T. I. 2013. Numerical simulation of charged particulate cluster-droplet impact on electrified surfaces. *Journal of Computational Physics*. **233**, 509-526.
25. Zohdi, T. I. 2012. Dynamics of charged particulate systems. Modeling, theory and computation. Springer-Verlag.

26. Zohdi, T. I. 2004. A computational framework for agglomeration in thermo-chemically reacting granular flows. *Proceedings of the Royal Society*. Vol. 460. Num. 2052, 3421-3445.
27. Zohdi, T. I. 2005. A simple model for shear stress mediated lumen reduction in blood vessels. *Biomechanics and Modeling in Mechanobiology*. Volume 4, Number 1, p57 - 61.
28. Zohdi, T. I. 2014. Mechanically-driven accumulation of microscale material at coupled solid-fluid interfaces in biological channels. *Proceedings of the Royal Society Interface*. 11, 20130922.
29. Zohdi, T. I., Holzapfel, G. A. and Berger, S. A. 2004. A phenomenological model for atherosclerotic plaque growth and rupture. *The Journal of Theoretical Biology*. Vol. 227, Issue 3, pp. 437-443.
30. Maxwell, J. C. 1867. On the dynamical theory of gases. *Philos. Trans. Soc. London*. **157**, 49.
31. Maxwell, J. C. 1873. A treatise on electricity and magnetism. 3rd. Ed. Clarendon Press, Oxford.
32. Rayleigh, J. W. 1892. On the influence of obstacles arranged in rectangular order upon properties of a medium. *Phil. Mag.* **32**, 481-491.
33. Jikov, V. V., Kozlov, S. M., Olenik, O. A. 1994. Homogenization of differential operators and integral functionals. Springer-Verlag.
34. Mura, T. 1993. Micromechanics of defects in solids, 2nd edition. Kluwer Academic Publishers.
35. Markov, K. Z. 2000. Elementary micromechanics of heterogeneous media. In *Heterogeneous Media: Micromechanics Modeling Methods and Simulations* (K. Z. Markov, and L. Preziosi, Eds.), pp. 1 162. Birkhauser, Boston.
36. Ghosh, S. 2011. Micromechanical Analysis and Multi-Scale Modeling Using the Voronoi Cell Finite Element Method. CRC Press/Taylor & Francis.
37. Ghosh, S. and Dimiduk, D. 2011. Computational Methods for Microstructure-Property Relations. Springer NY.
38. Abedian, B. and Kachanov, M. 2010. On the effective viscosity of suspensions *International Journal of Engineering Science*. 48(11):962965. DOI: 10.1016/j.ijengsci.2010.08.012
39. Sevostianov, I. and Kachanov, M. 2012. Effective properties of heterogeneous materials: Proper application of the non-interaction and the "dilute limit" approximations. *The International Journal of Engineering Science*. Volume 58, 124-128.

## 10 Appendix 1: Effective property bounds

The literature on methods to estimate the overall macroscopic properties of heterogeneous materials dates back at least to Maxwell [30,31] and Lord Rayleigh [32], with a notable contribution being the Hashin-Shtrikman bounds [18-20]. The Hashin-Shtrikman bounds are the tightest possible bounds on isotropic effective responses, generated from isotropic microstructures, where the volumetric data and phase contrasts of the constituents are the only data known. For linearized elasticity applications, for isotropic materials with isotropic effective (mechanical) responses, the Hashin-Shtrikman bounds (for a two-phase material) are as follows:

$$\kappa^{*,-} \stackrel{\text{def}}{=} \kappa_1 + \frac{\nu_2}{\frac{1}{\kappa_2 - \kappa_1} + \frac{3(1-\nu_2)}{3\kappa_1 + 4G_1}} \leq \kappa^* \leq \kappa_2 + \frac{1 - \nu_2}{\frac{1}{\kappa_1 - \kappa_2} + \frac{3\nu_2}{3\kappa_2 + 4G_2}} \stackrel{\text{def}}{=} \kappa^{*,+}, \quad (25)$$

and for the shear modulus

$$G^{*, -} \stackrel{\text{def}}{=} G_1 + \frac{\nu_2}{\frac{1}{G_2 - G_1} + \frac{6(1 - \nu_2)(\kappa_1 + 2G_1)}{5G_1(3\kappa_1 + 4G_1)}} \leq G^* \leq G_2 + \frac{(1 - \nu_2)}{\frac{1}{G_1 - G_2} + \frac{6\nu_2(\kappa_2 + 2G_2)}{5G_2(3\kappa_2 + 4G_2)}} \stackrel{\text{def}}{=} G^{*, +}, \quad (26)$$

where  $\kappa_2$  and  $\kappa_1$  are the bulk moduli and  $G_2$  and  $G_1$  are the shear moduli of the respective phases ( $\kappa_2 \geq \kappa_1$  and  $G_2 \geq G_1$ ), and where  $\nu_2$  is the second phase volume fraction. Such bounds are the tightest possible on isotropic effective responses, with isotropic two phase microstructures, where only the volume fractions and phase contrasts of the constituents are known. Note that no geometric or statistical information is required for the bounds. For an authoritative review of (a) the general theory of random heterogeneous media see, for example, Torquato [21], (b) for more mathematical homogenization aspects, see Jikov et al. [33], (c) for solid-mechanics inclined accounts of the subject see, for example, Hashin [20], Mura [34] or Markov [35]. We note that numerical methods have become the dominant tool to determining effective properties. In particular, Finite Element-based methods are extremely popular, and we refer the reader to Ghosh [36], Ghosh and Dimiduk [37] and Zohdi and Wriggers [15].

Finally, to derive Equation 15, one can take the limit of the particle phase becoming rigid, i.e. the bulk and shear moduli tending towards infinity,  $\kappa_p \rightarrow \infty$  and  $G_p \rightarrow \infty$ , signifying that the particles are much stiffer than the interstitial fluid, while simultaneously specifying that the interstitial fluid is incompressible, i.e.  $\kappa_f/G_f \rightarrow \infty$  with  $G_f$  being finite. This yields,

$$G^* = G_f \left(1 + 2.5 \frac{\nu_p}{1 - \nu_p}\right). \quad (27)$$

One can then assign  $\mu_f$  the value of  $G_f$  to obtain Equation 15. See, for example, Abedian and Kachanov [38] and Sevostianov and Kachanov [39] for more details.

## 11 Appendix 2: Reduction in failure strength due to voids

The failure of most structural materials is associated with reaching a critical deviatoric stress. In order to determine the reduction in failure strength due to voids, we denote the macroscopic effective elastic shear modulus as  $\mu^{*,voids}$  and the deviatoric stress at yield as  $\Sigma^{*,voids,t}$ . To start the analysis, we consider the dense material to have met the failure stress ( $\Sigma'_m$ ), thus yielding an expression for the overall failure stress ( $\Sigma^{*,voids,t}$ )

$$\langle \sigma' \rangle_{\Omega} = \nu_v \langle \sigma' \rangle_{\Omega_v} + \nu_m \langle \sigma' \rangle_{\Omega_m} = \nu_m \langle \sigma' \rangle_{\Omega_m} = (1 - \nu_v) \langle \sigma' \rangle_{\Omega_m} = (1 - \nu_v) \Sigma'_m = \Sigma^{*,voids,t}, \quad (28)$$

where  $\Sigma'_m$  is the stress at which the dense material fails. The effective shear modulus needed to determine  $\frac{\Sigma^{*,voids,t}}{2\mu^{*,voids}}$  can be estimated as in the the main

body of the text. Thus, for the small overall strains at which macroscopic failure occurs

$$2\mu^{*,voids} \langle \epsilon'_y \rangle_\Omega = 2\mu^{*,voids} \mathbf{Y}'^{*,voids} \approx 2\mu_m (1 - C(\nu_v)) \mathbf{Y}'^{*,voids} = \langle \sigma' \rangle_\Omega \approx \Sigma'_m (1 - \nu_v) \quad (29)$$

and thus

$$\mathbf{Y}'^{*,voids,*} = \left( \frac{\Sigma'_m}{2\mu_m} \right) \underbrace{\left( \frac{1 - \nu_v}{1 - \nu_v C(\nu_v)} \right)}_{\stackrel{\text{def}}{=} \Phi(\nu_v)}, \quad (30)$$

where  $\mathbf{Y}'^{*,voids,*}$  is the macroscopic small strain deviator at initial failure. Thus, we have

$$\mathbf{Y}'^{*,voids,*} \approx \frac{\Sigma^{*,voids,*}}{2\mu^{*,voids,*}} \approx \left( \frac{\Sigma'_m}{2\mu_m} \right) \Phi(\nu_v), \quad (31)$$

where the function  $\Phi(\nu_v)$  is a *slowly* increasing function of  $\nu_v$ . It is noted that since an upper bound was used in the construction of  $C(\nu_v)$ , and due to the functional dependence of  $\Phi$  on  $C(\nu_v)$ ,  $\Phi$  is an overestimation of the increase in the overall failure strain. One can then assign the effective properties of the slurry and binder to the matrix material,  $\mu^{*,no-voids,*} = \mu_m$ ,  $\Sigma'_m = \Sigma'^{*,no-voids,*}$  and  $\mathbf{Y}'_m = \mathbf{Y}'^{*,no-voids,*}$ . Thus, the change in the yield stress is

$$\Sigma'^{*,voids,*} = \Sigma'^{*,no-voids,*} (1 - \nu_v) \quad (32)$$

and the change in yield strain is

$$\mathbf{Y}'^{*,voids,*} \approx \left( \frac{\Sigma'^{*,no-voids,*}}{2\mu^{*,no-voids,*}} \right) \Phi(\nu_v) = \mathbf{Y}'^{*,no-voids,*} \Phi(\nu_v). \quad (33)$$